A lactate-dependent shift of glycolysis mediates synaptic and cognitive processes

Ignacio Fernández-Moncada[1]*, Unai B. Fundazuri[1,16], Gianluca Lavanco[1,2,15,16], Nasrin Bollmohr[1,16], Pauline Hachaguer[1], Tommaso Dalla Tor[1,2], Sarah Mountadem[1], Roman Serrat[1,3], Luigi Bellocchio[1], Astrid Cannich[1], Yusuke Nasu[4,5], Robert E. Campbell[4,6], Filippo Drago[2], Anne-Karine Bouzier-Sore[7], Luc Pellerin[8], Juan P. Bolaños[9,10,11], Gilles Bonvento[12], L. Felipe Barros[13,14], Stephane H. R. Oliet[1], Aude Panatier[1,17], Giovanni Marsicano[1,17,*]

[1]Université de Bordeaux, INSERM, Neurocentre Magendie, U1215, F-33000 Bordeaux, France.

[2]Department of Biomedical and Biotechnological Sciences, Section of Pharmacology, University of Catania, Catania 95124, Italy.

[3]INRAE, Nutrition and Integrative Neurobiology, UMR 1286, Bordeaux, France.

[4]Department of Chemistry, School of Science, The University of Tokyo, Bunkyo-ku, Tokyo 113-0033, Japan.

[5]PRESTO, Japan Science and Technology Agency, Chiyoda-ku, Tokyo 102-0075, Japan.

[6]Department of Chemistry, University of Alberta, Edmonton, AB T6G 2G2, Canada.

[7]Université de Bordeaux, CNRS, Centre de Résonance Magnétique des Systèmes Biologiques, UMR 5536, F-33000 Bordeaux, France.

[8]Université de Poitiers et CHU de Poitiers, INSERM, IRMETIST, U1313, Poitiers, France.

[9]Institute of Functional Biology and Genomics (IBFG), Universidad de Salamanca, CSIC, Salamanca, Spain.

[10]Institute of Biomedical Research of Salamanca (IBSAL), Hospital Universitario de Salamanca, Salamanca, Spain.

[11]Centro de Investigación Biomédica en Red de Fragilidad y Envejecimiento Saludable (CIBERFES), Madrid, Spain.

[12]Universite Paris-Saclay, CEA, CNRS, MIRCen, Laboratoire des Maladies Neurodegeneratives, Fontenay-aux-Roses, France.

[13]Centro de Estudios Cientificos, Valdivia, Chile.

[14]Universidad San Sebastián, Facultad de Medicina y Ciencia, Valdivia, Chile.

[15]Current address: Department of Health Promotion, Mother and Child Care, Internal Medicine and Medical Specialties, ''G. D'Alessandro'', University of Palermo. Palermo 90127, Italy.

[16]These authors contributed equally.

[17]These authors share senior authorship.

*Correspondence:

giovanni.marsicano@inserm.fr (G.M.)

ignacio.fernandez-moncada@inserm.fr (I.F-M.)

KEYWORDS

CB1 receptor, astrocytes, energy metabolism, lactate, serine, NMDAR, gliotransmission, neurotransmission

ABSTRACT

Control of brain energy metabolism and regulation of synaptic activity through gliotransmission are two important ways, through which astrocytes contribute to mental functions. However, the potential functional and molecular links between these two astrocyte-dependent processes have been scantly explored so far. Here we show that a lactate-dependent shift of glycolysis underlies the production of the gliotransmitter D-serine by acute activation of astrocyte type-1 cannabinoid (CB1) receptors, thereby gating synaptic and cognitive processes. Acute cannabinoid application causes a CB1 receptor-dependent rapid and reversible increase of lactate production and release in primary astrocyte cultures. As shown before, mutant mice lacking the CB1 receptor gene in astrocytes (GFAP-CB1-KO) were impaired in a novel object recognition (NOR) task. Notably, this phenotype was rescued not only by the gliotransmitter D-serine, but also by its precursor L-serine. Surprisingly, the administration of lactate also reverted the memory impairment of GFAP-CB1-KO mice. This rescue effect was abolished by *in vivo* blockade of the astrocyte-specific phosphorylated pathway (PP), which diverts glycolysis towards L-serine synthesis, suggesting that lactate itself might promote the accumulation of this amino acid. Consistent with this idea, lactate increased the co-agonist occupancy of CA1 post-synaptic hippocampal NMDA receptors in a PP-dependent manner. By establishing a mechanistic link between lactate, serine availability, synaptic activity and behavior, these results reveal an unforeseen functional connection between energy metabolism and gliotransmission to control cognitive processes.

MAIN

Type-1 cannabinoid (CB1) receptors are G-protein coupled receptors (GPCRs), that are prominently expressed across the central nervous system[1–3]. Physiological engagement of CB1 receptors by their endogenous ligands, the endocannabinoids, modulates many behavioral processes, including food intake, emotional responses and cognition[4]. Importantly, CB1 receptors can also be targeted by exogenous cannabinoids, such as Δ^9-tetrahydrocannabinol (THC), the main psychoactive component of *Cannabis sativa*. This exogenous, non-physiological activation might bear therapeutic properties, but it can also alter brain activity, impairing, for instance, cognitive, locomotor and perceptive functions[5]. Another remarkable feature of CB1 receptor signaling is its subcellular compartmentalization, which deviates from the strict plasma membrane functional localization of most GPCRs. Thus, few but functionally significant brain CB1 receptors are found in association with mitochondrial membranes (mtCB1 receptors), where they can alter mitochondrial functions and regulate behavior[6–10]. This uncommon subcellular distribution allows CB1 receptors to modulate brain functions *via* parallel signaling pathways triggered by specific subcellular pools[11].

CB1 receptors are highly expressed in neurons, but they are also present at low but functionally very relevant levels in other brain cell types, such as astrocytes[12]. Notably, astroglial CB1 receptors can govern brain functions and cognitive processes, such as novel object recognition (NOR)[13,14]. Recently, it has been shown that astrocytes also possess functional mtCB1 receptors[8,15,16]. In particular, persistent (24 hours) activation of mtCB1 receptors in astrocytes results in decreased mitochondrial functions and diminished lactate production. This astrocytic metabolic failure brings about neuronal stress and impairment of social behavior as observed 24 hours after cannabinoid exposure[16].

The present study originated from the idea of detailing the specific molecular underpinnings of such negative mtCB1 receptor-dependent control of brain lactate levels. However, early experiments lead to the surprising observation that short-term exposure to cannabinoid agonists can rapidly, reliably and transiently increase lactate

levels in astrocytes. Therefore, we set off to investigate the molecular mechanisms and the relevance of this observation. The results revealed a fully unexpected molecular link between metabolic and signaling properties of astrocytes, which can regulate physiological cognitive processes.

RESULTS

As previously shown using other methods[16], 24 hours stimulation of CB1 receptors lead to a reduction of lactate in cultured astrocytes expressing the reporter Laconic[17] (Extended Data Fig. 1A,B). With the original intention to investigate the temporal progression of this effect, we then analyzed the short-term impact of cannabinoid treatment. To our surprise, we observed that acute application of the CB1 agonist WIN55,212-2 (WIN55) was able to rapidly *increase* lactate levels in cultured astrocytes (Extended Data Fig. 1C,D). Therefore, we decided to investigate the mechanisms and the potential physiological and behavioral relevance of this phenomenon. Parallel cultures of astrocytes from wild-type (CB1-WT) and mutant CB1-KO mice expressing the reporter Laconic were shortly exposed to WIN55 (1 µM) and the fluorescent responses were imaged and quantified. We observed that the transient intracellular lactate increase induced by WIN55 was fully dependent on the presence of the CB1 receptor (Fig. 1A-C). The previously described negative effect of persistent CB1 agonism on lactate levels depends on mtCB1 receptors[16]. Thus, we tested if this specific subcellular pool was also involved in the short-term lactate increase induced by WIN55. Remarkably, this effect did not require mtCB1 receptors, as the lactate rise was not altered in astrocytes derived from DN22-CB1-KI mice, a genetic model lacking mitochondrial localization of CB1 receptors[7,18] (Fig. 1 A-C). Of note, the basal levels of lactate were not altered by the genotype of the astrocytes (Extended data Fig. 2A,B), and blockade of mitochondrial oxidative phosphorylation (OXPHOS) with sodium azide triggered similar lactate increases in CB1-WT, CB1-KO and DN22-CB1-KI astrocytes (Extended data Fig. 2C,D). This indicates that the differential effects of WIN55 on these cells could not be ascribed to differences in their basal levels of lactate or to their general ability to accumulate this metabolite.

Absolute intracellular increases of lactate can be due to enhanced production, but also to decreased release. To dissect these components in the acute effects of cannabinoid on lactate dynamics, we measured astrocyte lactate production *via* a transport-stop technique[17,19]. The effect of the broad monocarboxylate transporter (MCT) inhibitor Diclofenac[20,21] (Fig. 1D) is fully reversible (Extended data Fig. 2E). This

allows devising a paired assessment of lactate production by measuring the rate of accumulation upon MCT block, before and during WIN55 application (Fig. 1E). Stimulation of CB1 receptors in WT astrocytes resulted in a significant increase in the rate of intracellular lactate accumulation, indicating augmented lactate production (Fig. 1E,F). To exert its physiological functions, lactate is extruded from astrocytes into the extracellular space[22,23]. Thus, we next asked whether the WIN55-induced lactate production was accompanied with increased release of the metabolite. To explore this possibility, we adapted a “sniffer cells” strategy[24,25], in which HEK cells expressing an extracellular lactate fluorescent biosensor[26] are able to detect the amount of ambient lactate levels in an extracellular medium (Fig. 1G), in the presence of a constant buffer superfusion. Whereas WIN55 did not alter the extracellular lactate levels in a pure culture of sniffer cells, its application to a co-culture of sniffer cells with CB1-WT astrocytes led to an extracellular lactate accumulation (Fig. 1H,I). Importantly, extracellular lactate remained unchanged upon WIN55 exposure when sniffers cells were mixed with CB1-KO astrocytes (Fig. 1H,I).

Altogether, these data indicate that, opposite to the persistent negative effects involving mitochondrial CB1 receptor signaling[16], short-term activation of non-mitochondrial associated astroglial CB1 receptors results into the transient stimulation of lactate production and release.

To determine if the quick stimulation of lactate metabolism mediated by astroglial CB1 receptors is relevant for brain functions, we took advantage of the known role of endocannabinoid signaling in the novel object recognition (NOR) task[14]. Mice lacking CB1 receptors in cells expressing the astrocyte marker glial fibrillary acidic protein (GFAP-CB1-KO mice)[27] are impaired in NOR performance[14]. This phenotype has been explained by lack of hippocampal synaptic D-serine availability and consequent impairment of N-Methyl-D-Aspartate Receptors (NMDAR) function during the consolidation phase of the task[14]. Notably, it is not known if this physiological control of NOR performance depends on the mitochondrial pool of astroglial CB1 receptors. To address this point, we used a specific double-viral rescue approach to delete astroglial CB1 receptors and re-express either the CB1-WT or the DN22-CB1 proteins in the

hippocampus of CB1-floxed mice[8,11,14,28], thereby generating Control, HPC-GFAP-CB1-KO, HPC-GFAP-CB1-RS and HPC-GFAP-DN22-CB1-RS mice, respectively (see Methods and Fig 2A). As expected[14], the deletion of CB1 receptors from hippocampal astrocytes resulted in impaired NOR performance (Fig 2B). Remarkably, this impairment of HPC-GFAP-CB1-KO mice was rescued by either re-expression of wild-type CB1 and mutant DN22-CB1 in HPC-GFAP-CB1-RS and HPC-GFAP-DN22-CB1-RS, respectively (Fig 2B and Extended data Fig 3), indicating that mtCB1 receptor signaling is not necessary for physiological endocannabinoid-dependent control of NOR performance.

The data collected so far show that non-mitochondrial astroglial CB1 receptors can both increase lactate accumulation and mediate physiological NOR performance. Considering that efficient lactate metabolism is required for several behavioral processes[22,29], we asked whether this metabolic function of astroglial CB1 receptors might contribute determining the synaptic activity required for NOR performance. A post-training intraperitoneal (I.P.) injection of lactate at a concentration known to reach the brain parenchyma (1 g/kg)[30], was able to fully rescue the NOR impairment of GFAP-CB1-KO mice (Fig. 3A and Extended data Fig. 4A). As this rescue effect was very similar to the one obtained with D-serine[14], we hypothesized that astroglial CB1 receptor control of lactate might participate in the regulation of synaptic D-serine levels to provide physiological NOR performance. D-serine is an amino acid derived from L-serine[31–34], which, in the brain, is produced exclusively by astrocytes *via* the consumption of the glycolytic intermediate 3-phosphoglycerate (3PG) in the phosphorylated pathway[31] (Fig. 3B). To test whether astroglial CB1 receptor-dependent increase of lactate might impact L-serine activity in the brain, we first assessed the potential impact of L-serine on astroglial CB1 receptor-dependent NOR performance. An I.P. injection of L-serine (0.5 g/kg) was also able to rescue the memory deficit of GFAP-CB1-KO mice (Fig. 3A and Extended data Fig. 4A), suggesting that the impaired D-serine availability in these mutants[14] might be ascribed to a decreased astrocytic L-serine production. To address this idea and identify the potential relationship between lactate and serine signaling, we adopted a pharmacological approach to inhibit phosphoglycerate dehydrogenase (PHGDH), the enzyme providing the first step of L-serine production in the phosphorylated pathway[31] (Fig. 3B). The administration of high doses of the PHGDH

blocker NCT-503 (Fig. 3C; Ref. 35) alone impaired NOR consolidation, possibly due to direct inhibition of L- and D-serine availability (Extended data Fig. 4B,C). Thus, we performed a full dose-response study to identify a sub-effective dose of NCT-503 that does not alter memory formation *per se* (Extended data Fig. 4B,C). Then, we tested the ability of lactate to rescue the memory impairment of GFAP-CB1-KO mice under vehicle or in the presence of this dose (6 mg/kg). Whereas NCT-503 administration did not alter the memory formation of GFAP-CB1-WT mice or the memory impairment of their GFAP-CB1-KO littermates, the drug fully abolished the lactate-induced rescue of NOR performance in GFAP-CB1-KO mice (Fig. 3D and Extended data Fig. 4D). Importantly, the delivery of L-serine was still able to rescue the memory impairment in the presence of the same dose of NCT-503 (Fig. 3D and Extended data Fig 4D), indicating that the action of L-serine was downstream of the PHGDH activity. Overall, these results suggest that the physiological activation of astroglial CB1 receptors enables cognitive performance *via* stimulation of glucose metabolism, increase of lactate supply, and potentiation of L- and D-serine availability *via* the phosphorylated pathway.

These results suggest that lactate might control synaptic D-serine availability, eventually resulting in the adequate signaling of NMDARs. However, it is still possible that the mechanisms underlying the rescue effect of lactate in the NOR performance of GFAP-CB1-KO mice are explained by compensatory mechanisms developed under the specific conditions of the mutant mice. In other words, the deletion of the CB1 gene in astrocytes might induce alterations that provide lactate with functions that it does not have under physiological conditions. To address this point and to clarify the role of lactate levels on the dynamics of synaptic D-serine, we explored if the link between these metabolites as observed in the GFAP-CB1-KO mice is also present in WT animals. As a proxy indicator of the synaptic levels of D-serine, we performed electrophysiological extracellular field recordings to study the co-agonist binding site occupancy of synaptic NMDARs in the CA1 region of WT hippocampal slices[14,34]. Intriguingly, bath application of exogenous lactate (2 mM) was able to potentiate NMDAR activity with a magnitude similar to the one induced by exogenous D-serine (Fig. 4A). However, this lactate-induced potentiation was slower than the one triggered by D-serine (Fig. 4B and Extended data Fig. 5A,B), consistent with the idea that the effect of lactate is likely not

explained by a direct action at NMDAR. To test whether this lactate effect was downstream the increase in D-serine availability, the co-agonist binding sites of synaptic NMDARs were first saturated with exogenous D-serine (50 µM) and then lactate was bath applied. Notably, lactate application had no impact on NMDAR activity in these conditions (Fig. 4C and Extended data Fig 5C), suggesting that its potentiating effect might be due to a downstream increase in D-serine availability. However, it is still possible that the application of D-serine might cause a "ceiling effect", impeding a serine-independent effect of lactate to be observed. Therefore, we directly tested whether the activity of the phosphorylated pathway was necessary for the potentiation on NMDAR signalling by lactate. Strikingly, this effect was blunted in slices preincubated with NCT-503 (Fig. 4D and Extended data Fig 5D), showing that PHGDH activity is a required step of the process. Of note, the potentiation induced by D-serine was not altered by NCT-503 (Extended data Fig 5E), further suggesting that lactate plays an upstream role in the astrocyte cascade leading to D-serine co-agonism at NMDARs.

These results confirm that lactate can modulate the phosphorylated pathway to control synaptic D-serine availability independently of CB1 receptor genetic deletion, supporting a physiological role for this phenomenon.

DISCUSSION

This study reveals a novel astrocyte-dependent metabolic interaction between lactate, the phosphorylated pathway, synaptic D-serine availability and cognitive performance in mice. This process is controlled by astroglial CB1 receptors, adding a new layer of complexity to the signaling of the endocannabinoid system in the brain and highlighting a mechanistic connection between astrocytic energy metabolism and gliotransmission. Thus, our data are compatible with a scheme whereupon endogenous activation of astroglial CB1 receptors leads to acute increase of lactate, which in turn switches glycolysis towards serine production, ultimately providing the NMDAR activity necessary for novel object recognition.

Astroglial CB1 receptors have been shown to control synaptic plasticity in different brain regions and to determine cognitive processes[12,14,36–38]. The regulation of astrocyte calcium signaling is generally indicated as the cellular mechanism underlying these functions[39–41]. Only recently, cannabinoid signaling was linked to specific metabolic control of behavior, showing that persistent activation of astroglial mtCB1 receptors can reduce lactate levels and social interactions[16]. Here, using lactate-sensitive fluorescent biosensors, we confirmed that long-term application of cannabinoids reduces lactate levels in astrocytes[16], but we found also that short-term activation of astroglial CB1 receptors stimulates lactate production and release. Consistent with this observation, the exogenous administration of lactate is sufficient to rescue the NOR impairment of GFAP-CB1-KO mice. Lactate levels increase in the brain parenchyma during neural workload[42], a phenomenon explained by a shift from complete to partial glucose oxidation and known as aerobic glycolysis[43]. Several signals have been proposed to initiate this metabolic shift, such as glutamate[44,45], extracellular K^+ rises[46,47] and others[24,48,49]. The present data indicate that astroglial CB1 receptor signaling participates in these processes, suggesting that it can trigger aerobic glycolysis and concomitant increase in extracellular lactate levels. When compared to other brain signals, the effect of CB1 receptor activation on lactate metabolism share a similar time scale to the effects of extracellular K^+ rises, which activate astrocyte glycolysis within seconds[50,51] and promote a phenomenon of metabolic recruitment of neighboring

astrocytes[47]. However, endocannabinoid signaling is thought to be highly local[52], a characteristic similar to glutamate which does not diffuse far from its release sites[53]. This suggests that CB1 receptors may provide fast and local signaling to trigger astrocyte lactate metabolism, working in parallel or synergistically with other brain signals that control astrocyte metabolic functions. Many studies showed that astrocyte-borne lactate is necessary for correct memory formation, mostly by acting as a metabolic substrate for neurons[54–58]. Our results add to this idea the possibility that lactate might promote cognitive processes also by a novel mechanism involving D-serine signaling.

Noteworthy, our present and previous[16] data indicate that activation of CB1 receptors likely results in a biphasic time-dependent modulation of astrocyte lactate metabolism. We previously showed that persistent pharmacological activation (24 hours) of astroglial mtCB1 receptors decreases lactate production, thereby causing neuronal bioenergetic stress and impairing social interactions in mice[16]. Conversely, in the present study, we report that a short-term activation (< 10 min) of non-mitochondrial astrocyte CB1 receptors results in a transient increase of intracellular lactate. This bimodal and subcellular-specific action on lactate levels resembles the recently described differential involvement of neuronal plasma membrane and mitochondrial CB1 receptors in cannabinoid-induced antinociception and catalepsy, respectively[11]. However, those subcellular-specific effects of cannabinoids occur simultaneously, whereas the differential impact on lactate levels seems to involve an important temporal component. Future studies will address the molecular mechanisms underlying this switch between non-mitochondrial and mitochondrial effects of CB1 receptors on lactate levels and its functional consequences. In this context, it is also interesting to note that the physiological control of NOR performance and its pharmacological impairment by cannabinoid agonists seem to rely on very different molecular pathways. Thus, whereas exogenous cannabinoids impair NOR behavior through the activation of mtCB1 receptors[7], the present data show that mitochondrial localization of the receptor is not necessary to assure physiological NOR performance. The potential differential effect of mitochondrial and non-mitochondrial CB1 receptors on lactate metabolism might play a role in this apparent discrepancy between physiological and pharmacological (endo)cannabinoid actions. Future studies will address this intriguing possibility.

Lactate has traversed a long way from being initially viewed as little more than mere cellular waste, to become a relevant metabolite for brain physiology[22,42]. Astrocyte-derived lactate has been shown to modulate neuronal functions *via* multiple mechanisms[59–67]. Most of these proposed mechanisms, however, are linked to the role of lactate as an energy substrate for neuronal activity. In contrast, the present data add an unforeseen and not strictly energetic mode of action of lactate on brain functions: the control of D-serine synthesis and its synaptic availability. This process requires the activity of the phosphorylated pathway, an astrocyte-exclusive metabolic cascade[31,34]. This novel metabolic process likely works in parallel with the other described effects of lactate in the brain, allowing astrocytes to use a single metabolite both to potentiate and to maintain neuronal functions, and thus minimizing the resources required to cater active neurons.

An open question is how lactate modulates the phosphorylated pathway to promote L-serine synthesis. Currently, we do not have an answer to this question. However, some possibilities can already be speculated upon: (i) Lactate might activate allosterically[68], post-translationally[69] or through a receptor-mediated mechanisms[22] the enzymes of the phosphorylated pathway involved in the L-serine synthesis, (ii) Lactate might promote glucose-serine conversion by inhibiting the transformation of 3PG into pyruvate, or (iii) Lactate might be used as a direct substrate for the synthesis of serine. Alongside these hypothetical mechanisms, the spatio-temporal pattern of lactate-stimulated L-serine activity might also play a potentially important role. It is possible that the CB1-dependent increase of lactate and the production of L-serine coexist in a single astrocyte, but they are separated in time. In other words, upon CB1 receptor activation, astrocytes may first accumulate lactate and then use it to promote L-serine. Alternatively, CB1 receptor-stimulated astrocytes might act as net lactate providers, whereas another astrocyte population may possibly be responsible for the L-serine production upon stimulation by lactate. This possibility might be similar to the specific gating of striatal circuits by distinctive astrocyte subpopulations[70], and the recently proposed secondary metabolic recruitment induced by the diffusion of lactate away from its release site[47]. Further focused studies will be necessary to fully unveil the potential mechanisms explaining the metabolic interaction between lactate and L-serine. However, the discovery of the

existence of such interaction reveals key connections between metabolic (lactate) and synaptic (D-serine) signaling, which are required for cognitive processes.

D-Serine is a gliotransmitter and co-agonist of synaptic NMDARs[14,34,71–73]. Despite that both neurons and astrocytes can likely release this amino acid[32,38], astrocytes are the main producers of its precursor L-serine[33], thereby representing the main controllers of the total amount of D-serine in the brain. By showing that astrocyte-borne lactate promotes D-serine signaling *via* stimulation of L-serine by the phosphorylated pathway, our results underscore another way by which astrocytes modulate brain functions. Thus, this study contributes to a unifying concept of astrocyte metabolic functions and gliotransmission. These two processes are often considered as independent entities. For instance, some researchers see astrocytes as pure "metabolic" processors and others consider them purely as sources of synaptic signaling control[74–77], with little interactions between these points of view. This is particularly true when the roles of astrocytes are investigated in the frame of cognition and high mental processes. In this study, we merged the new observation that type-1 cannabinoid CB1 receptors can rapidly and transiently promote lactate metabolism and the regulation of D-serine synaptic functions by endocannabinoid signaling in astrocytes, thereby showing the tight functional link existing between metabolic and signaling processes. This unified notion will have to be taken into account in future studies on the role of astrocytes in promoting and controlling brain function and behavior.

ACKNOWLEDGEMENTS

We would like to thank Delphine Gonzales, Nathalie Aubailly, Ruby Racunica, Jean-Baptiste Bernard and all the personnel of the Animal Facilities of the NeuroCentre Magendie for mouse care. We also thank the genotyping platform of the Neurocentre Magendie for the help in the experiments. The microscopy was done in the Bordeaux Imaging Center a service unit of the CNRS-INSERM and Bordeaux University, member of the national infrastructure France BioImaging supported by the French National Research Agency (ANR-10-INBS-04). We thank all past and present members of

Marsicano's lab for useful discussions and for their invaluable support. This study was funded by Inserm (to G.M., A.P. and S.H.R.O.); CNRS (to A.P. and S.H.R.O.); the European Research Council (Micabra, ERC-2017-AdG-786467, to G.M.); Fondation pour la Recherche Medicale (DRM20101220445, to G.M); EMBO Long-term Fellowship ALTF87-2018 (to I.F-M.); the Human Frontiers Science Program (to G.M.); Region Aquitaine (CanBrain, AAP2022A-2021-16763610 and -17219710 to A.-K.B.-S., L.P., A.P. and G.M.); French State/Agence Nationale de la Recherche (CaCoVi, ANR 18-CE16-0001-02; MitObesity, ANR 18-CE14-0029-01; ERA-Net Neuron CanShank, ANR-21-NEU2-0001-04, to G.M), (BrainFuel, ANR-21-CE44-0023-01 to A.-K.B.-S., L.P and AP.), (Excigly, ANR-20-CE16-0009-03 to S.H.R.O.), (Astrocom ANR-19-CE16-0015 to A.P.), (ANR-19-CE14-0039 to L.B.); University of Bordeaux's IdEx "Investments for the Future" program / GPR BRAIN_2030, the Japan Society for the Promotion of Science (21K14738, to Y.N. and 19H05633, to R.E.C.) and the Japan Science and Technology Agency (JPMJPR22E9, to Y.N.), Fondation Alzheimer (to G.B.), the NextGenerationEU/PRTR and Agencia Estatal de Investigación (10.13039/501100011033; PID2019-105699RB-I00; PDC2021-121013-I00; RED2018-102576-T, to JP.B); Instituto de Salud Carlos III (CB16/10/00282, to JP.B), Junta de Castilla y León (CS/151P20 and Escalera de Excelencia CLU-2017-03 to JP.B), European Comission action HORIZON-TMA-MSCA-DN (ETERNITY, 101072759, to JP.B), Fondecyt 1200029 & BMBF-ANID 180045 (to L.F.B.).

AUTHORS CONTRIBUTION

IFM conceived the study, wrote the manuscript and performed most experiments; UBF, GL and NB performed behavioral and electrophysiological experiments; PH, TDT, SM, RS, LB and AC helped with experiments; YN and REC generated and provided sensor constructs; FD, AKBS, LP, JPB, GB, LFB and SHRO provided theoretical support and ideas; AP conceived the study; GM conceived the study and wrote the manuscript; all authors edited and approved the manuscript.

DECLARATION OF INTERESTS

Authors declares no conflict of interest.

FIGURE LEGENDS

Figure 1. Acute stimulation of astrocytes lactate metabolism by CB1 receptors.

A, Subcellular localization of CB1 receptors in the primary astrocytes culture models. **B**, Intracellular lactate measurement during exposure to WIN55 (1 µM), in CB1-WT (blue circles, average of 42 cells), CB1-KO (white circles, average of 29 cells) and DN22-CB1-KI (red circles, average of 42 cells) astrocytes. **C**, Quantification of lactate change after 5 min exposure to WIN55. CB1-WT: n=7, 247 cells. CB1-KO: n=7, 252 cells. DN22-CB1-KI: n=6, 235 cells. **D**, Transport stop protocol for measurement of lactate production. Diclofenac is a broad inhibitor of monocarboxylate transporter (MCT) activity. The blockade of MCT causes an intracellular lactate accumulation that is proportional to its rate of production. **E**, Measurement of lactate production before and during exposure to WIN55 (1 µM). The production rate is indicated with a solid line above the corresponding lactate accumulation. **F**, Summary of the lactate production rates before (pale blue circles) and during exposure to WIN55 (grey circles), computed from experiments similar to panel E. N=4, 102 cells. **G**, Sniffer cell strategy for determination of extracellular lactate levels. HEK cells expressing an extracellular lactate fluorescent biosensor (sniffers cells) were cultured alone or in co-culture with astrocytes. **H**, Extracellular lactate measurements during exposure to WIN55 (1 µM), in a pure culture of sniffers cells (yellow circles, average of 81 cells), a co-culture of sniffers cells and CB1-WT astrocytes (green circles, average of 76 cells) and a co-culture of sniffers cells and CB1-KO astrocytes (white circles, average of 102 cells). **I**, Quantification of the extracellular lactate level after 10 min exposure to WIN55. Sniffer culture: n=3, 406 cells. Sniffer + CB1-WT astrocytes co-culture: n=7, 997 cells. Sniffer + CB1-KO astrocytes co-culture: n=4, 469 cells. Data corresponds to a single experiment average (mean±SEM) (**B**,**H**). Result corresponds to a representative cell (**E**). Circles in scatter or before-after plots correspond to individual cells (**C**,**F**,**I**). Bars correspond to experiments average (mean±SEM), with circles representing individual experiment average (**C**,**F**,**I**). Statistical analysis was performed using a Kruskal-Wallis test followed by Dunn's multiple comparison test (**A**), two-tailed paired t-test (**F**) and One-way ANOVA followed by Tukey's multiple comparison test (**I**).

Figure 2. The astroglial mtCB1 receptor is not necessary for physiological NOR performance.

A, Schematic of the viral approach used for deletion of hippocampal astroglial CB1 receptors and expression rescue with either wild type or DN22-CB1 sequences. Four groups of animals; Control, HPC-GFAP-CB1-KO, HPC-GFAP-CB1-RS and HPC-GFAP-DN22-CB1-RS mice; were obtained by *s*tereotactic injection of a mix of specific AAV constructs (see material and methods for details). **B**, Summary of NOR performance in Control (blue), HPC-GFAP-CB1-KO (white), HPC-GFAP-CB1-RS (teal) and HPC-GFAP-DN22-CB1-RS (red) mice, n= 7-9 mice per condition. Bars correspond to experiments average (mean±SEM) and circles represent individual animals (**B**). Statistical analysis was performed using a One-way ANOVA followed by Tukey's multiple comparison test (**B**).

Figure 3. Lactate promotes NOR performance *via* the phosphorylated pathway.

A, NOR performance of GFAP-CB1-WT (blue circles) and GFAP-CB1-KO (white circles) mice. Animals were treated either with an I.P. injection of vehicle, lactate (1 g/kg) or L-serine (0.5 g/kg), immediately after the acquisition phase. N= 13-23 mice per condition. **B**, Scheme depicting the lactate production and the phosphorylated pathway, and its interaction at the level of 3-phosphoglycerate (3PG). **C**, Scheme depicting the expected effect of a sub-effective dose of NCT-503 on the L-serine synthesis. **D**, NOR performance of GFAP-CB1-WT (blue circles) and GFAP-CB1-KO (white circles) mice. Animals were treated either with an I.P. injection of vehicle + NCT-503 (6 mg/kg), lactate (1 g/kg) + NCT-503 or L-serine (0.5 g/kg) + NCT-503, immediately after the acquisition phase. N= 6-16 mice per condition. Bars correspond to experiments average (mean±SEM) and circles represent individual animals (**A**,**D**). Statistical analysis was performed using a two-way ANOVA (**A**,**D**).

Figure 4. Synaptic D-serine availability is modulated by lactate.

A, Summary plot showing the effect of exogenous D-serine (50 µM – magenta circles, n=5) or lactate (2 mM – green circles, n=9) on NMDAR-mediated fEPSPs slopes in acute hippocampal slices from WT animals. The representative NMDAR-fEPSPs traces (on the right) are the average of 20 successive sweeps before (in black) and after exogenous application of D-serine (in pink) or lactate (in green). **B**, Increase rate of the NMDAR-mediated fEPSPs potentiation, obtained by fitting a non-linear function to the data presented in panel A. See Extended Fig 4A for more details. **C** Summary plot of NMDAR-fEPSPs slopes before (magenta circles) and during lactate exposure (2 mM – magenta/green circles, n=6) in slices preincubated with D-serine (50 µM)**.** The representative NMDAR-fEPSPs traces (on top) are the average of 20 successive sweeps before (in black) and after exogenous application of lactate (in green) in the presence of D-serine since the beginning of the experiment. **D**, NMDAR- fEPSPs slopes before (grey circles) and during bath application of D-serine (50 µM – magenta circles, n=4) or lactate (2 mM – green circles, n=5), in slices preincubated with NCT-503 (10-20 µM). Data are presented as mean±SEM (**A**,**C**,**D**). Bars correspond to experiments average (mean±SEM) and circles represent single measurement (**B**). Statistical analysis was performed using a two-tailed unpaired t-test (**B**) and a two-way ANOVA test (**A**,**C**,**D**).

Extended Data Figures legends

Extended Data Figure 1 – Differential effect of cannabinoids on astrocyte lactate level.

A, Intracellular lactate imaging in astrocytes previously incubated with WIN55 (2 μM) or vehicle (DMSO) for 24 hours. After treatment, and to determine the basal lactate level (occupancy), cells were imaged and exposed sequentially to an OXPHOS blocker (5 mM sodium azide), pyruvate (10 mM) and lactate (10 mM). R_0, basal ratio. R_{min}, minimum ratio. R_{max}, maximum ratio. Data was normalized to R_{min} to emphasize the difference in R_0. **B**, Basal lactate level (occupancy) after 24 hours treatment with WIN55 (2 μM) or vehicle (DMSO). Data was computed as occupancy = $(R_0-R_{min})/(R_{max}-R_{min})$, using R_0, R_{min} and R_{max} from experiments similar to panel A. Vehicle, n=3, 26 cells. WIN55, n=3, 25 cells. **C**, Intracellular lactate imaging in astrocytes acutely exposed to WIN55 (2 μM). BL = baseline. **D**, Summary of intracellular lactate level at baseline (BL) and after 3 min exposure to WIN55 (2 μM), in experiments similar to Extended Data Fig 1C, n=3, 26 cells. Data correspond to representative cells (**A**,**C**). Circles in scatter and before-after plots correspond to single cells (**B**,**D**). Statistical analysis was performed using a two-tailed unpaired t-test (**B**) and two-tailed paired t-test (**D**).

Extended Data Figure 2 – The basal lactate level and accumulation upon mitochondria inhibition is not altered by CB1 receptor subcellular localization.

A, Intracellular lactate imaging in astrocytes. To determine the basal lactate level (occupancy), cells exposed sequentially to WIN55 (1 μM), OXPHOS block (5 mM azide), Oxamate (6 mM) and AR-C155858 (1 μM). R_0, basal ratio. R_{min}, minimum ratio. R_{max}, maximum ratio. Average of 4 independent experiments. Cells: WT=158, KO=145, DN22=154. **B**, Basal lactate level (occupancy) in CB1-WT, CB1-KO and DN22-CB1-KI astrocytes. Data was computed as occupancy = $(R_0-R_{min})/(R_{max}-R_{min})$, using R_0, R_{min} and R_{max} obtained from experiments similar to panel A. N = 4, cells analyzed: CB1-WT=158, CB1-KO=145, DN22-CB1-KI =154. **C**, Intracellular lactate accumulation induced by

OXPHOS block (5 mM sodium azide). Average of several cells in a representative experiment (CB1-WT=42, CB1-KO=29, DN22-CB1-KI =42 cells). **D**, Summary of intracellular lactate levels after 2 min of OXPHOS block (5 mM sodium azide), in experiments similar to those shown in panel C. CB1-WT: n=7, 247 cells. CB1-KO: n=7, 252 cells. DN22-CB1-KI: n=6, 235 cells. **E**, Summary of two sequential measurements of basal lactate production with diclofenac. N=4, 95 cells analyzed. Data corresponds to the experiments average and represented as mean±SEM (**A**,**C**). Circles in scatter and before-after plots correspond to single cells (**B**,**D**,**E**). Bars correspond to experiments average (mean±SEM) and circles represent individual experiment average (**B**,**D**). Statistical analysis was performed using Kruskal-Wallis test followed by Dunn's multiple comparison test (**B**), One-way ANOVA followed by Tukey's multiple comparison test (**D**) and two-tailed paired t-test (**E**).

Extended Data Figure 3 – NOR exploration time impairment can be rescued either by expressing the CB1 wild type or DN22-CB1 mutant sequence.

A, Exploration times of familiar versus novel objects in the NOR task, from Control (blue lines), GFAP-CB1-KO (black lines), GFAP-CB1-WT-RS (teal lines) and GFAP- DN22-CB1-RS (red lines) animals, n = 7-9 mice per condition. A single line corresponds to an individual animal

Extended Data Figure 4 – Inhibition of the phosphorylated pathway impairs NOR consolidation in WT mice and in lactate-treated GFAP-CB1-KO mice.

A, Exploration time of familiar versus novel objects in the NOR task of GFAP-CB1-WT (blue lines) and GFAP-CB1-KO mice (black lines) mice, treated either with vehicle (veh), 1 g/kg lactate (Lac) or 0.5 g/kg L-serine (L-Ser), immediately after the acquisition phase. GFAP-CB1-WT, n=13-18 animals. GFAP-CB1-KO, n= 15-23 animals. **B**, NOR performance in wild-type mice treated either with vehicle or incremental doses of NCT-503. n=7-15 mice per condition. **C**, Exploration time of familiar versus novel object in the

NOR task of wild-type mice treated either with vehicle or incremental doses of NCT-503. n= 7-15 mice per condition. **D**, Exploration time of familiar versus novel object in the NOR task, of mice treated either with vehicle + 6 mg/kg NCT-503 (NCT), 1 g/kg lactate + 6 mg/kg NCT-503 (NCT + Lac) or 0.5 g/kg L-serine + 6 mg/kg NCT-503 (NCT + L-Ser), immediately after the acquisition phase. GFAP-CB1-WT mice (blue lines), n=6-12 animals. GFAP-CB1-KO mice (black lines), n= 9-16 animals. A single line corresponds to an individual animal (**A**, **C**, **D**). Data is presented as scatter plot with the line and whisker corresponding to the mean±SEM and circles to individual animals (**B**). Statistical analysis was performed with a One-way ANOVA followed by Tukey's multiple comparison test (**B**).

Extended Data Figure 5 – Lactate, but not D-serine, requires the phosphorylated pathway to potentiate NMDAR function.

A, Non-linear model and equation used to analyze the data shown in Fig 3A. The fitted parameters can be used to determine the increase rate of the curve and the ΔPotentiation. **B**, ΔPotentiation induced by lactate and D-serine computed with the parameters obtained from the non-linear fit of the data presented in Fig3A. **C,** Potentiation induced by lactate (2 mM) in slices preincubated with D-serine (50 µM). Data corresponds to the quantification of NMDAR- fEPSP slopes from the experiment shown in Fig. 2C, n=6. **D**, NMDAR-mediated fEPSP slopes in the presence of lactate (same as Fig 1A, n=9) and lactate + NCT-503 (n=5). **E**, NMDAR- fEPSP slopes induced by D-serine (same as Fig 1A, n=5) and D-serine after NCT-503 preincubation (n=4). Bars correspond to experiments average (mean±SEM) and circles represent individual experiment average (**B**, **C**). Data corresponds to the experiments average and represented as mean±SEM. Data point were averaged every 5 mins (**D**,**E**). Statistical analysis was performed using a two-way ANOVA (**D**,**E**).

MATERIAL AND METHODS

Animals.

All experiments were conducted in strict compliance with the European Union recommendations (2010/63/EU) and were approved by the French Ministry of Agriculture and Fisheries (authorization number 3306369) and the local ethical committee (authorization APAFIS#18111). Animals used in the study were divided into two categories. The first group consisted of female and male CB1-KO, CB1-DN22 or CB1-WT mice, used as breeders to obtain newborn mice for primary cultures. The second category correspond to animals used for behavior or electrophysiology studies, consisting of male C57BL/6N (JANVIER, France), male $CB1^{f/f}$, male GFAP-CB1-KO mutant and GFAP-CB1-WT littermate mice (two to three months-old). Animals were housed in groups under standard conditions, with free access to food and water, in a day/night cycle of 12/12 hr (light on at 7 am). Specific deletion of CB1 on GFAP positive cells in adult mice was obtained via loxP/Cre system, with a tamoxifen inducible CreERT2 recombinase[78] encoded under the GFAP promoter[27]. Female mice carrying the ‘‘floxed’’ CB1 gene ($CB1^{f/f}$)[79] were crossed with $CB1^{f/f;GFAP\text{-}CreERT2}$, to obtain $CB1^{f/f;GFAP\text{-}CreERT2}$ and $CB1^{f/f}$ littermates, named throughout the text GFAP-CB1-KO and GFAP-CB1-WT, respectively. For induction of CB1 deletion, 7-9 weeks-old mice were treated daily with 1 mg tamoxifen via intraperitoneally (i.p.) injections (10 mg/mL dissolved in 90% sesame oil, 10% ethanol) for 8 days. After each injection, mice were surveilled and weighted every two days to control their wellbeing. Mice were used 3-5 weeks after the last tamoxifen injection[14,27].

Surgery and viral stereotaxic injection.

Male $CB1^{f/f}$ (CB1-flox) mice were anesthetized in a box containing 5% Isoflurane (Virbac, France) before being placed in a stereotaxic frame (Model 900, Kopf Instruments, CA, USA) in which 1.5% to 2.0% of Isoflurane was continuously supplied via an anesthetic mask during the whole duration of the experiment. For viral intra-hippocampal AAV delivery, mice were submitted to stereotaxic surgery and AAV vectors were injected with the help of a microsyringe (0.25 mL Hamilton syringe with a 30-gauge beveled needle)

attached to a pump (UMP3-1, World Precision Instruments, FL, USA). Where specified, CB1-flox mice were injected directly into the hippocampus (HPC) (0.5 µL per injection site at a rate of 0.5 µL per min), with the following coordinates: HPC, AP -1.8; ML ± 1; DV -2.0 and -1.5. Following virus delivery, the syringe was left in place for 1 minute before being slowly withdrawn from the brain. To induce the deletion of hippocampal astroglial CB1 receptors and the rescue (RS) of CB1 receptor expression either with WT or mutant DN22 sequences, mice were injected in the hippocampus with the following combination of viral particles: (i) AAV-CAG-DIO-empty + AAV-GFAP-GFP (Control mice), (ii) AAV-GFAP-CRE-GFP + AAV-CAG-DIO-empty (HPC-GFAP-CB1-KO mice), (iii) AAV-GFAP-CRE-GFP + AAV-CAG-DIO-CB1 (HPC-GFAP-CB1-RS mice) and (iv) AAV-GFAP-CRE-GFP + AAV-CAG-DIO-DN22-CB1 (HPC-GFAP-DN22-CB1-RS mice). Animals were used around 4-5 weeks after local AAV infusions. Mice were weighed daily and individuals that failed to regain the pre-surgery body weight were excluded from the behavioral experiments.

Mixed cortical brain cell cultures.

Mixed cortical cultures of neuronal and glial cells were prepared from 1 to 3-day-old neonatal mice as previously described[80]. Briefly, mice were euthanized, the brain removed, and cortex dissected in iced cold Hank's balanced salt solution. The tissue was enzymatically digested with trypsin/EDTA for 5 min at 37 °C and the enzymatic digestion was stopped with 10% FBS in B-27 supplemented neurobasal medium. After this, a gently dissociation of the tissue was performed by repeatedly passing it through a 1-mL micropipette tip. Obtained cells were left in suspension to allow debris precipitation and removal. Cells were seeded in 18-mm glass coverslips treated with poly-L-lysine and incubated for 90 min to allow cell adhesion. After this, medium was replaced with fresh B-27 supplemented neurobasal medium with 10 mM glucose, 0.24 mM pyruvate, 2 mM GlutaMAX^{TM,} 100 U/mL penicillin, 100 µg/mL streptomycin and 2.5 µg/mL amphotericin B at 37 °C in a humidified atmosphere of 5% CO_2. At day in vitro (DIV) 13–14, cultures were exposed to 1×10^6 plaque forming units (pfu) of adenoviral vectors (serotype 5) coding for Laconic[17]. Measurements were carried out 48-72 h after

infection of cells (DIV 16-17). Adenoviral vectors encoding the FRET biosensor were custom made by Vector Biolabs (PA, USA).

Cell lines.

HEK293T cells (ATCC, CRL-3216TM, lot 62729596) were cultured in Dulbecco's modified Eagle's medium (DMEM) with 1 g/L glucose, supplemented with 10% fetal bovine serum (FBS), 100 U/mL penicillin, and 100 µg/mL streptomycin, 0.1 mM of Gibco® MEM Non-Essential Amino Acids, and maintained at 37 °C in a humidified atmosphere of 5% CO_2. For "sniffers cells" experiments, cells were transfected 18 - 24 hours before experiments with 1 µg plasmid DNA encoding for the extracellular lactate fluorescent biosensor eLACCO2.1 (Ref. 26), using polyethylenimine (PEI) as transfection agent. On the day of experiment, the DMEM media was replace for B-27 supplemented neurobasal (used for the mixed glia-neuron culture) and cells were detached gently with a micropipette. Immediately after, the cell suspension was seeded on mixed glia-neuron and incubated for 4 - 5 hours before imaging.

Drug preparation and administration.

For in vitro experiments, water soluble drugs were dissolved directly in the imaging solution (see below for its composition). Concentrated stocks of drugs prepared in DMSO were diluted directly in the imaging solution. The imaging solution contained the same amount of solvent respectively to the drug(s). For behavioral experiments, sodium lactate and L-serine were prepared in saline (0.9% NaCl). NCT-503 was prepared in a mixture of saline with 2.5% cremophor and 2.5% DMSO to obtain a solution of 0.6 mg/ml. All drugs were injected i.p. with a 26G needle, immediately after the acquisition phase of the NOR task (see below), and in the following order: first an injection of NCT-503 or vehicle, followed by a 5 min pause and then an injection of vehicle, lactate or L-serine. Vehicles contained the same amounts of solvents respectively to the drug. All drugs were prepared fresh before the experiments.

Fluorescence imaging.

Mixed cortical glia-neuron cultures, HEK293T cells or a co-culture of mixed glia-neuron culture with HEK293 cells (sniffers), were mounted in an open chamber and imaged on wide-field mode with an inverted Leica DMI 6000 microscope (Leica Microsystems, Wetzlar, Germany) equipped with a resolutive HQ2 camera (Photometrics, Tucson, USA). The illumination system used was a lumencor spectra 7 (Lumencor, Beaverton, USA). The objectives used were a HC PL APO CS 20X dry 0.7 NA and a HCX PL APO CS 40X oil 1.25 NA. Multi-positions were done with a motorized stage Scan IM (Märzhäuser, Wetzlar, Germany). A 37°C atmosphere was created with an incubator box and an air heating system (Life Imaging Services, Basel, Switzerland). The system was controlled by MetaMorph software (Molecular Devices, Sunnyvale, USA). Cells were superfused with an imaging solution consisting of (in mM): 10 HEPES, 112 NaCl, 24 $NaHCO_3$, 3 KCl, 1.25 $MgCl_2$, 1.25 $CaCl_2$, 2 glucose, 0.5 sodium lactate and bubbled with air/5% CO_2 at 37 °C, at a constant flow of 3 mL/min. Astrocytes expressing Laconic were imaged at 40X, and excited at 430 nm for 0.01–0.05 s, emissions collected at 465-485 nm for mTFP and 542-556 nm for Venus, with image acquisition every 10 s. The ratio between mTFP and Venus was computed and normalized to the baseline. To quantify the basal lactate level (Extended Data Fig. 1A-B and Extended Data Fig. 2A-B), the biosensor occupancy was computed as a proxy of intracellular lactate level with the following equation: Occupancy = $(R_0-R_{min})/(R_{max}-R_{min})$, in which R_0: basal mTFP/Venus ratio (before any drug treatment), R_{min}: steady state mTFP/Venus ratio induced by sodium oxamate (6 mM) or pyruvate (10 mM), R_{max}: steady state mTFP/Venus ratio obtained after MCTs block (1 µM AR-C155858) or 10 mM lactate. Lactate production rates (Fig. 1 E-F) were computed by fitting a linear rate to the first minutes of lactate accumulation during MCTs block with 0.5 mM diclofenac. HEK293 cells expressing eLACCO2.1 (either alone or in co-culture) were imaged at 20X, excited at 475 nm for 0.05–0.1 s and emission collected at 509-547 nm for GFP, with image acquisition every 10 s. The obtained GFP fluorescence was normalized to the baseline.

Novel Object Recognition Memory Task.

The novel object recognition (NOR) test took place in a L-shaped maze as previously described[14,81]. The behavior task was carried out in a room adjacent to mice housing with a light intensity of 50 ± 3 lux. An overhung video camera over the maze was used to record mice behavior and scoring was performed offline. The task consisted of 3 sequential daily trials of 9 min each. On day 1, the habituation phase, mice were placed in the center of the maze and allowed to freely explore the arms in the absence of any objects. On day 2, the acquisition phase, mice were placed in the center of the maze with the presence of two identical objects positioned at the extremities of each arm and left to freely explore the maze and the objects. On day 3, the long-term memory test phase (24 hours after acquisition session), similarly to day 2, mice were placed in the center of the maze with two objects but one of the familiar objects was replaced by a novel object of different shape, color, and texture, and mice were left to explore both objects. The position of the novel object and the associations of novel and familiar were randomized. All objects were previously tested to avoid biased preference. The apparatus as well as objects were cleaned before experimental use and between each animal testing with water and at the end of experimental session with ethanol 70%. Cognitive performance was assessed by the discrimination index (DI), computed as the difference between the time spent exploring the novel (TN) and the familiar object (TF) divided by the total exploration time (TN+TF): DI = [TN-TF]/[TN+TF]. Object exploration was defined as the nose-poking of the objects. Mice with a total exploration time <15 s were not included in the data analysis. Memory performance was also evaluated by directly comparing the exploration time of novel and familiar objects, respectively. Experienced investigators evaluating the exploration were blind to the treatment and/or genotype of the animals. Normally, mice carried out the task without issues, however some mice performed behaviors incompatible with the test (i.e., not exploring both objects, either by chance or due peeing in a maze arm and refusing to cross over the urine.) These mice were returned to the home cage and retested one hour after. If mice failed again to perform the behavioral task, they were excluded from the experiment.

Electrophysiology.

Slice preparation

After being anaesthetized with 5% isoflurane for two minutes, mice were decapitated, and the brain quickly extracted in ice-cold artificial cerebrospinal fluid (aCSF) containing (in mM): 125 NaCl, 2.5 KCl, 1 $NaH2PO_4$, 1.2 $MgCl_2$, 0.6 $CaCl_2$, 26 $NaHCO_3$ and 11 Glucose (pH 7.3, 305 mosmol/kg). Coronal hippocampal slices (350 µm) were prepared using a vibratome (Leica VT1200 S) and hemisected. Next, Slices were incubated in aCSF containing 2 mM MgCl2 and 1 mM CaCl2 during 30 minutes at 33°C. Finally, slices were allowed to rest for 1h at room temperature before starting recordings.

NMDAR field excitatory postsynaptic potentials recordings

Slices were transferred into a recording chamber and perfused continuously with aCSF (3 mL/min) containing this time 1.3 mM MgCl2 and 2.5 mM CaCl2. Field excitatory postsynaptic potentials (fEPSPs) were recorded with a Multiclamp 700B amplifier (Axon Instruments, Inc.) using pipettes (2-4 MΩ) filled with aCSF and placed in the *stratum radiatum* of the CA1 area. NMDA-fEPSPs were isolated with low Mg^{2+} aCSF (0.2 mM) in the presence of 2,3-dihydroxy-6-nitro-7-sulfamoyl-benzo[f]quinoxaline-2,3-dione (NBQX) (10 µM) to block AMPA/kainate receptors, respectively. The stimulation of the Schaffer collaterals (0.05 Hz, 100 µs duration) with a concentric bipolar tungsten electrode was used to induce synaptic responses. Recorded signals were filtered at 2 kHz and digitized at 10 kHz via a DigiData 1440 (Axon Instruments, Inc.). Data were collected and analyzed offline using pClamp 10.7 software (Axon Instruments Inc.).

Average NMDAR-fEPSPs traces were recorded from at least 20 min of stable recordings. Lactate (2 mM) or D-serine (50 µM) were bath applied 20 min before the recording and then during the whole experiment. To determine if both metabolites act through the same pathway an occlusion experiment was also performed during which the impact of lactate was tested in the presence of D-serine present from the beginning of the experiment. Finally, we tested whether lactate act through a mechanism coupled to the D-serine synthesis pathway. Thus, the impact of both exogenous lactate and D-

serine on NMDA receptor-mediated fEPSPs was recorded in the presence of the PHGDH inhibitor, NCT-503 (10-20 µM). The effects of all tested molecules on NMDA-mediated fEPSPs were recorded at least for 40 minutes after drug application.

Quantification and statistical analysis.

All graphs, linear regressions and statistical analyses were performed using GraphPad software (version 8 or 9). Data is presented as time course (average of imaged cells ± SEM, from a representative experiment), scatter plots of individual cells and bars + symbols. In some experimental data, the SEM is small enough to be contained inside symbols. Otherwise, time courses without error bars correspond to a representative cell from an independent experiment and is indicated in the figure legend. All data was analyzed for outliers using the ROUT method (false discovery rate of 1%), and for normality with the Shapiro Wilk test. To perform the statistical analysis, the electrophysiology data was averaged every 5 min. Differences between groups were assessed using the average of each independent experiment using either by paired t-test, unpaired t-test, one-way ANOVA followed by Tukey's multiple comparison test, Kruskal-Wallis followed by Dunn's multiple comparison test or two-way ANOVA followed by Tukey's multiple comparison test. $P < 0.05$ was considered significant and are annotated in each figure. Otherwise, nonsignificant data is indicated as NS.

REFERENCES

1. Busquets-Garcia, A., Bains, J. & Marsicano, G. CB1 Receptor Signaling in the Brain: Extracting Specificity from Ubiquity. *Neuropsychopharmacol.* **43**, 4–20 (2018).
2. Zou, S. & Kumar, U. Cannabinoid Receptors and the Endocannabinoid System: Signaling and Function in the Central Nervous System. *Int J Mol Sci* **19**, 833 (2018).
3. Martinez Ramirez, C. E. *et al.* Endocannabinoid signaling in the central nervous system. *Glia* **71**, 5–35 (2023).
4. Busquets-Garcia, A. *et al.* Dissecting the cannabinergic control of behavior: The where matters. *BioEssays* **37**, 1215–1225 (2015).
5. Stella, N. THC and CBD: Similarities and differences between siblings. *Neuron* S0896-6273(22)01119–9 (2023) doi:10.1016/j.neuron.2022.12.022.
6. Benard, G. *et al.* Mitochondrial CB(1) receptors regulate neuronal energy metabolism. *Nat Neurosci* **15**, 558–564 (2012).
7. Hebert-Chatelain, E. *et al.* A cannabinoid link between mitochondria and memory. *Nature* **539**, 555–559 (2016).
8. Serrat, R. *et al.* Astroglial ER-mitochondria calcium transfer mediates endocannabinoid-dependent synaptic integration. *Cell Rep* **37**, 110133 (2021).
9. Robledo-Menendez, A., Vella, M., Grandes, P. & Soria-Gomez, E. Cannabinoid control of hippocampal functions: the where matters. *FEBS J* **289**, 2162–2175 (2022).
10. Jong, Y.-J. I., Harmon, S. K. & O'Malley, K. L. Intracellular GPCRs Play Key Roles in Synaptic Plasticity. *ACS Chem Neurosci* **9**, 2162–2172 (2018).
11. Soria-Gomez, E. *et al.* Subcellular specificity of cannabinoid effects in striatonigral circuits. *Neuron* **109**, 1513-1526.e11 (2021).

12. Covelo, A., Eraso-Pichot, A., Fernández-Moncada, I., Serrat, R. & Marsicano, G. CB1R-dependent regulation of astrocyte physiology and astrocyte-neuron interactions. *Neuropharmacology* **195**, 108678 (2021).
13. Ramon-Duaso, C., Conde-Moro, A. R. & Busquets-Garcia, A. Astroglial cannabinoid signaling and behavior. *Glia* (2022) doi:10.1002/glia.24171.
14. Robin, L. M. *et al.* Astroglial CB1 Receptors Determine Synaptic D-Serine Availability to Enable Recognition Memory. *Neuron* **98**, 935-944.e5 (2018).
15. Gutiérrez-Rodríguez, A. *et al.* Localization of the cannabinoid type-1 receptor in subcellular astrocyte compartments of mutant mouse hippocampus. *Glia* **66**, 1417–1431 (2018).
16. Jimenez-Blasco, D. *et al.* Glucose metabolism links astroglial mitochondria to cannabinoid effects. *Nature* **583**, 603–608 (2020).
17. San Martín, A. *et al.* A genetically encoded FRET lactate sensor and its use to detect the Warburg effect in single cancer cells. *PLoS ONE* **8**, e57712 (2013).
18. Soria-Gomez, E. *et al.* Habenular CB1 Receptors Control the Expression of Aversive Memories. *Neuron* **88**, 306–313 (2015).
19. Barros, L. F. *et al.* Small is fast: astrocytic glucose and lactate metabolism at cellular resolution. *Front Cell Neurosci* **7**, 27 (2013).
20. Contreras-Baeza, Y. *et al.* Monocarboxylate transporter 4 (MCT4) is a high affinity transporter capable of exporting lactate in high-lactate microenvironments. *J. Biol. Chem.* **294**, 20135–20147 (2019).
21. Sasaki, S. *et al.* Effect of diclofenac on SLC16A3/MCT4 by the Caco-2 cell line. *Drug Metab Pharmacokinet* **31**, 218–223 (2016).

22. Magistretti, P. J. & Allaman, I. Lactate in the brain: from metabolic end-product to signalling molecule. *Nat Rev Neurosci* **19**, 235–249 (2018).
23. Zuend, M. *et al.* Arousal-induced cortical activity triggers lactate release from astrocytes. *Nat Metab* **2**, 179–191 (2020).
24. Lerchundi, R. *et al.* NH4(+) triggers the release of astrocytic lactate via mitochondrial pyruvate shunting. *Proc. Natl. Acad. Sci. U.S.A.* **112**, 11090–11095 (2015).
25. Sotelo-Hitschfeld, T. *et al.* Channel-mediated lactate release by K+-stimulated astrocytes. *The Journal of Neuroscience* **35**, 4168–4178 (2015).
26. Nasu, Y. *et al.* Improved genetically encoded fluorescent biosensors for monitoring of intra- and extracellular L-lactate. 2022.12.27.522013 Preprint at https://doi.org/10.1101/2022.12.27.522013 (2022).
27. Han, J. *et al.* Acute cannabinoids impair working memory through astroglial CB1 receptor modulation of hippocampal LTD. *Cell* **148**, 1039–1050 (2012).
28. Oliveira da Cruz, J. F. *et al.* Specific Hippocampal Interneurons Shape Consolidation of Recognition Memory. *Cell Rep* **32**, 108046 (2020).
29. Veloz Castillo, M. F., Magistretti, P. J. & Calì, C. l-Lactate: Food for Thoughts, Memory and Behavior. *Metabolites* **11**, 548 (2021).
30. Carrard, A. *et al.* Peripheral administration of lactate produces antidepressant-like effects. *Mol Psychiatry* **23**, 488 (2018).
31. Maugard, M., Vigneron, P.-A., Bolaños, J. P. & Bonvento, G. l-Serine links metabolism with neurotransmission. *Prog Neurobiol* **197**, 101896 (2021).
32. Coyle, J. T., Balu, D. & Wolosker, H. D-Serine, the Shape-Shifting NMDA Receptor Co-agonist. *Neurochem Res* **45**, 1344–1353 (2020).

33. Neame, S. *et al.* The NMDA receptor activation by d-serine and glycine is controlled by an astrocytic Phgdh-dependent serine shuttle. *Proceedings of the National Academy of Sciences* **116**, 20736–20742 (2019).
34. Le Douce, J. *et al.* Impairment of Glycolysis-Derived l-Serine Production in Astrocytes Contributes to Cognitive Deficits in Alzheimer's Disease. *Cell Metabolism* **31**, 503-517.e8 (2020).
35. Pacold, M. E. *et al.* A PHGDH inhibitor reveals coordination of serine synthesis and one-carbon unit fate. *Nat Chem Biol* **12**, 452–458 (2016).
36. Araque, A., Castillo, P. E., Manzoni, O. J. & Tonini, R. Synaptic functions of endocannabinoid signaling in health and disease. *Neuropharmacology* **124**, 13–24 (2017).
37. Oliveira, J. F. & Araque, A. Astrocyte regulation of neural circuit activity and network states. *Glia* **70**, 1455–1466 (2022).
38. Sherwood, M. W., Oliet, S. H. R. & Panatier, A. NMDARs, Coincidence Detectors of Astrocytic and Neuronal Activities. *International Journal of Molecular Sciences* **22**, 7258 (2021).
39. Savtchouk, I. & Volterra, A. Gliotransmission: Beyond Black-and-White. *J Neurosci* **38**, 14–25 (2018).
40. Durkee, C. A. & Araque, A. Diversity and Specificity of Astrocyte-neuron Communication. *Neuroscience* **396**, 73–78 (2019).
41. Papouin, T., Dunphy, J., Tolman, M., Foley, J. C. & Haydon, P. G. Astrocytic control of synaptic function. *Philos Trans R Soc Lond B Biol Sci* **372**, (2017).

42. Barros, L. F. Metabolic signaling by lactate in the brain. *Trends Neurosci.* **36**, 396–404 (2013).
43. Barros, L. F. *et al.* Aerobic Glycolysis in the Brain: Warburg and Crabtree Contra Pasteur. *Neurochem Res* (2020) doi:10.1007/s11064-020-02964-w.
44. Pellerin, L. & Magistretti, P. J. Glutamate uptake into astrocytes stimulates aerobic glycolysis: a mechanism coupling neuronal activity to glucose utilization. *Proc Natl Acad Sci U S A* **91**, 10625–10629 (1994).
45. Zimmer, E. R. *et al.* [18F]FDG PET signal is driven by astroglial glutamate transport. *Nat Neurosci* **20**, 393–395 (2017).
46. Fernández-Moncada, I. *et al.* Neuronal control of astrocytic respiration through a variant of the Crabtree effect. *Proc Natl Acad Sci U S A* **115**, 1623–1628 (2018).
47. Barros, L. F., Ruminot, I., Sotelo-Hitschfeld, T., Lerchundi, R. & Fernández-Moncada, I. Metabolic Recruitment in Brain Tissue. *Annu Rev Physiol* (2022) doi:10.1146/annurev-physiol-021422-091035.
48. San Martín, A., Arce-Molina, R., Galaz, A., Pérez-Guerra, G. & Barros, L. F. Nanomolar nitric oxide concentrations quickly and reversibly modulate astrocytic energy metabolism. *J. Biol. Chem.* **292**, 9432–9438 (2017).
49. Mazucanti, C. H., Kawamoto, E. M., Mattson, M. P., Scavone, C. & Camandola, S. Activity-dependent neuronal Klotho enhances astrocytic aerobic glycolysis. *J Cereb Blood Flow Metab* **39**, 1544–1556 (2019).
50. Bittner, C. X. *et al.* Fast and reversible stimulation of astrocytic glycolysis by K+ and a delayed and persistent effect of glutamate. *J. Neurosci.* **31**, 4709–4713 (2011).

51. Ruminot, I. *et al.* NBCe1 mediates the acute stimulation of astrocytic glycolysis by extracellular K+. *J. Neurosci.* **31**, 14264–14271 (2011).
52. Dudok, B. & Soltesz, I. Imaging the endocannabinoid signaling system. *J Neurosci Methods* **367**, 109451 (2022).
53. Jensen, T. P. *et al.* Multiplex imaging relates quantal glutamate release to presynaptic Ca2+ homeostasis at multiple synapses in situ. *Nat Commun* **10**, 1414 (2019).
54. Suzuki, A. *et al.* Astrocyte-neuron lactate transport is required for long-term memory formation. *Cell* **144**, 810–823 (2011).
55. Newman, L. A., Korol, D. L. & Gold, P. E. Lactate produced by glycogenolysis in astrocytes regulates memory processing. *PLoS One* **6**, e28427 (2011).
56. Gao, V. *et al.* Astrocytic β2-adrenergic receptors mediate hippocampal long-term memory consolidation. *Proc Natl Acad Sci U S A* **113**, 8526–8531 (2016).
57. Netzahualcoyotzi, C. & Pellerin, L. Neuronal and astroglial monocarboxylate transporters play key but distinct roles in hippocampus-dependent learning and memory formation. *Prog Neurobiol* **194**, 101888 (2020).
58. Roumes, H. *et al.* Lactate transporters in the rat barrel cortex sustain whisker-dependent BOLD fMRI signal and behavioral performance. *Proc Natl Acad Sci U S A* **118**, e2112466118 (2021).
59. Bouzier-Sore, A.-K., Voisin, P., Canioni, P., Magistretti, P. J. & Pellerin, L. Lactate is a preferential oxidative energy substrate over glucose for neurons in culture. *J Cereb Blood Flow Metab* **23**, 1298–1306 (2003).

60. Bouzier-Sore, A.-K. *et al.* Competition between glucose and lactate as oxidative energy substrates in both neurons and astrocytes: a comparative NMR study. *Eur J Neurosci* **24**, 1687–1694 (2006).
61. Wyss, M. T., Jolivet, R., Buck, A., Magistretti, P. J. & Weber, B. In vivo evidence for lactate as a neuronal energy source. *J Neurosci* **31**, 7477–7485 (2011).
62. Hung, Y. P., Albeck, J. G., Tantama, M. & Yellen, G. Imaging cytosolic NADH-NAD(+) redox state with a genetically encoded fluorescent biosensor. *Cell metabolism* **14**, 545–54 (2011).
63. Yang, J. *et al.* Lactate promotes plasticity gene expression by potentiating NMDA signaling in neurons. *Proc Natl Acad Sci U S A* **111**, 12228–12233 (2014).
64. Herrera-López, G. & Galván, E. J. Modulation of hippocampal excitability via the hydroxycarboxylic acid receptor 1. *Hippocampus* **28**, 557–567 (2018).
65. Jorwal, P. & Sikdar, S. K. Lactate reduces epileptiform activity through HCA1 and GIRK channel activation in rat subicular neurons in an in vitro model. *Epilepsia* **60**, 2370–2385 (2019).
66. Briquet, M. *et al.* Activation of lactate receptor HCAR1 down-modulates neuronal activity in rodent and human brain tissue. *J Cereb Blood Flow Metab* **42**, 1650–1665 (2022).
67. Bozzo, L., Puyal, J. & Chatton, J.-Y. Lactate modulates the activity of primary cortical neurons through a receptor-mediated pathway. *PLoS One* **8**, e71721 (2013).
68. Costa Leite, T., Da Silva, D., Guimarães Coelho, R., Zancan, P. & Sola-Penna, M. Lactate favours the dissociation of skeletal muscle 6-phosphofructo-1-kinase

tetramers down-regulating the enzyme and muscle glycolysis. *Biochem J* **408**, 123–130 (2007).

69. Hagihara, H. *et al.* Protein lactylation induced by neural excitation. *Cell Rep* **37**, 109820 (2021).
70. Martín, R., Bajo-Grañeras, R., Moratalla, R., Perea, G. & Araque, A. Circuit-specific signaling in astrocyte-neuron networks in basal ganglia pathways. *Science* **349**, 730–734 (2015).
71. Panatier, A. *et al.* Glia-derived D-serine controls NMDA receptor activity and synaptic memory. *Cell* **125**, 775–784 (2006).
72. Papouin, T. *et al.* Synaptic and extrasynaptic NMDA receptors are gated by different endogenous coagonists. *Cell* **150**, 633–646 (2012).
73. Sherwood, M. W., Arizono, M., Panatier, A., Mikoshiba, K. & Oliet, S. H. R. Astrocytic IP3Rs: Beyond IP3R2. *Front Cell Neurosci* **15**, 695817 (2021).
74. Akther, S. & Hirase, H. Assessment of astrocytes as a mediator of memory and learning in rodents. *Glia* **70**, 1484–1505 (2022).
75. Hirrlinger, J. & Nimmerjahn, A. A perspective on astrocyte regulation of neural circuit function and animal behavior. *Glia* **70**, 1554–1580 (2022).
76. Lyon, K. A. & Allen, N. J. From Synapses to Circuits, Astrocytes Regulate Behavior. *Front Neural Circuits* **15**, 786293 (2021).
77. Fernández-Moncada, I. & Marsicano, G. Astroglial CB1 receptors, energy metabolism, and gliotransmission: an integrated signaling system? *Essays Biochem* EBC20220089 (2023) doi:10.1042/EBC20220089.

78. Hirrlinger, P. G., Scheller, A., Braun, C., Hirrlinger, J. & Kirchhoff, F. Temporal control of gene recombination in astrocytes by transgenic expression of the tamoxifen-inducible DNA recombinase variant CreERT2. *Glia* **54**, 11–20 (2006).
79. Marsicano, G. *et al.* CB1 cannabinoid receptors and on-demand defense against excitotoxicity. *Science* **302**, 84–88 (2003).
80. Bittner, C. X. *et al.* High resolution measurement of the glycolytic rate. *Front Neuroenergetics* **2**, (2010).
81. Da Cruz, J. F. O. *et al.* An Alternative Maze to Assess Novel Object Recognition in Mice. *Bio Protoc* **10**, e3651 (2020).

Fernandez-Moncada et al Figure 1

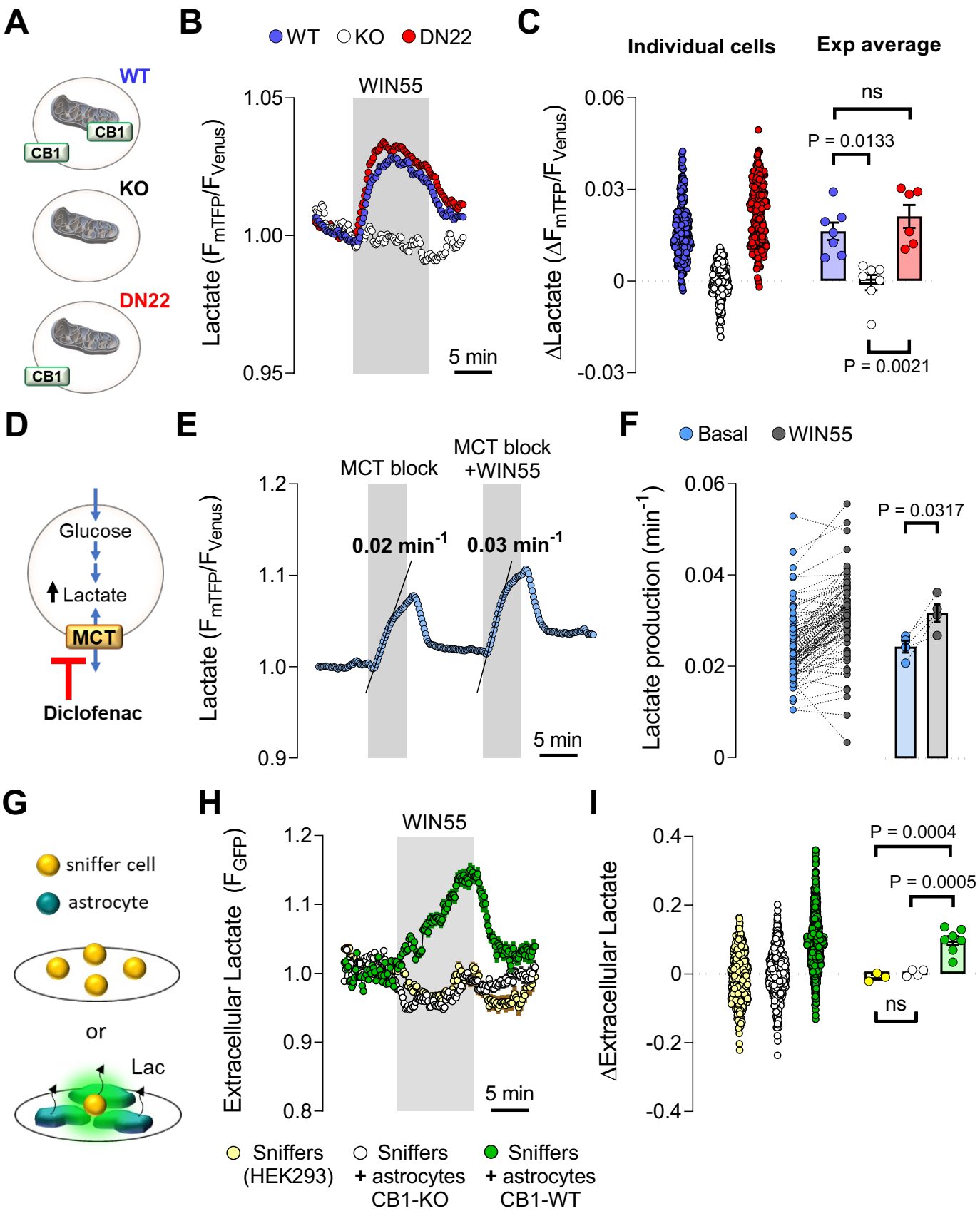

Fernandez-Moncada et al Figure 2

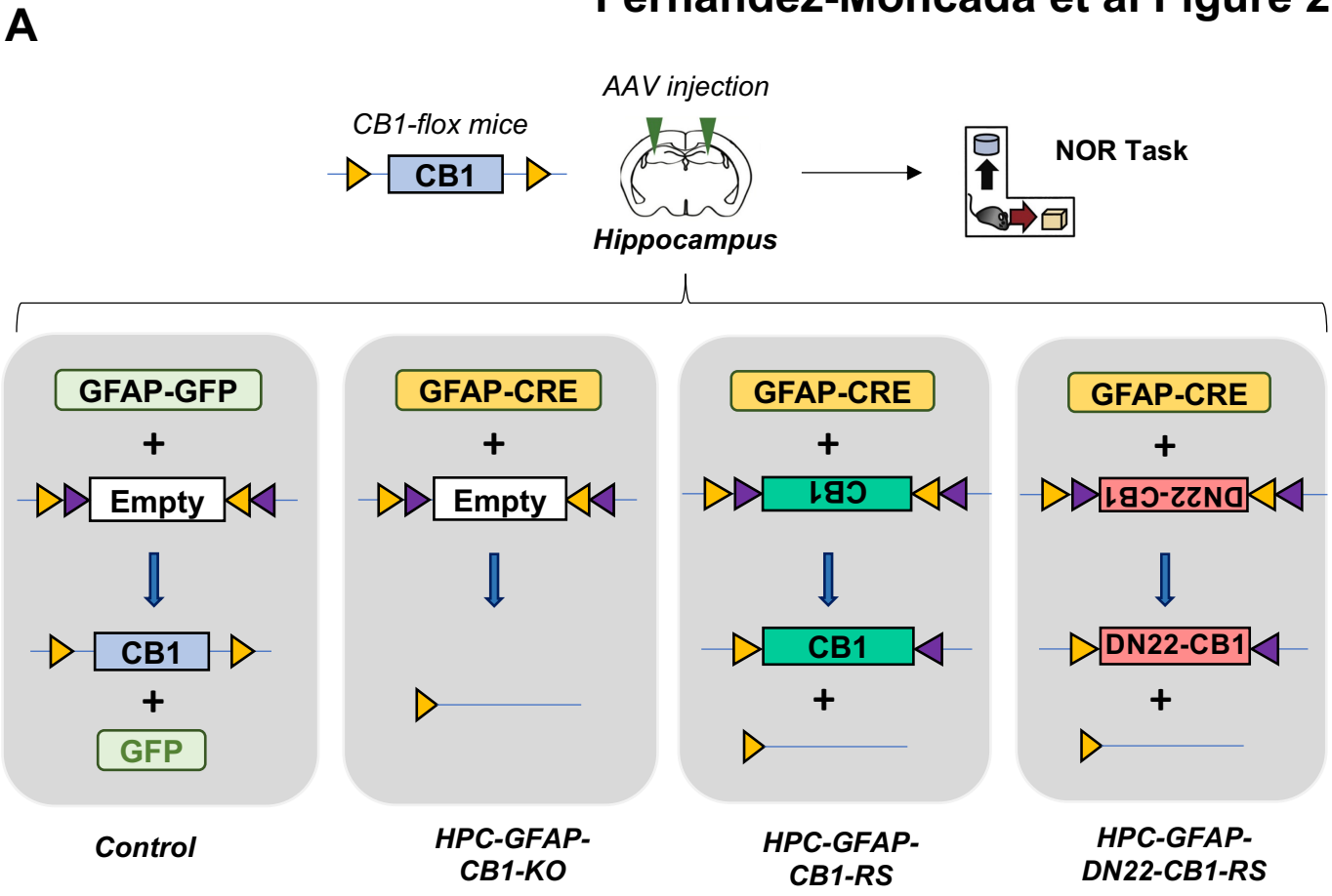

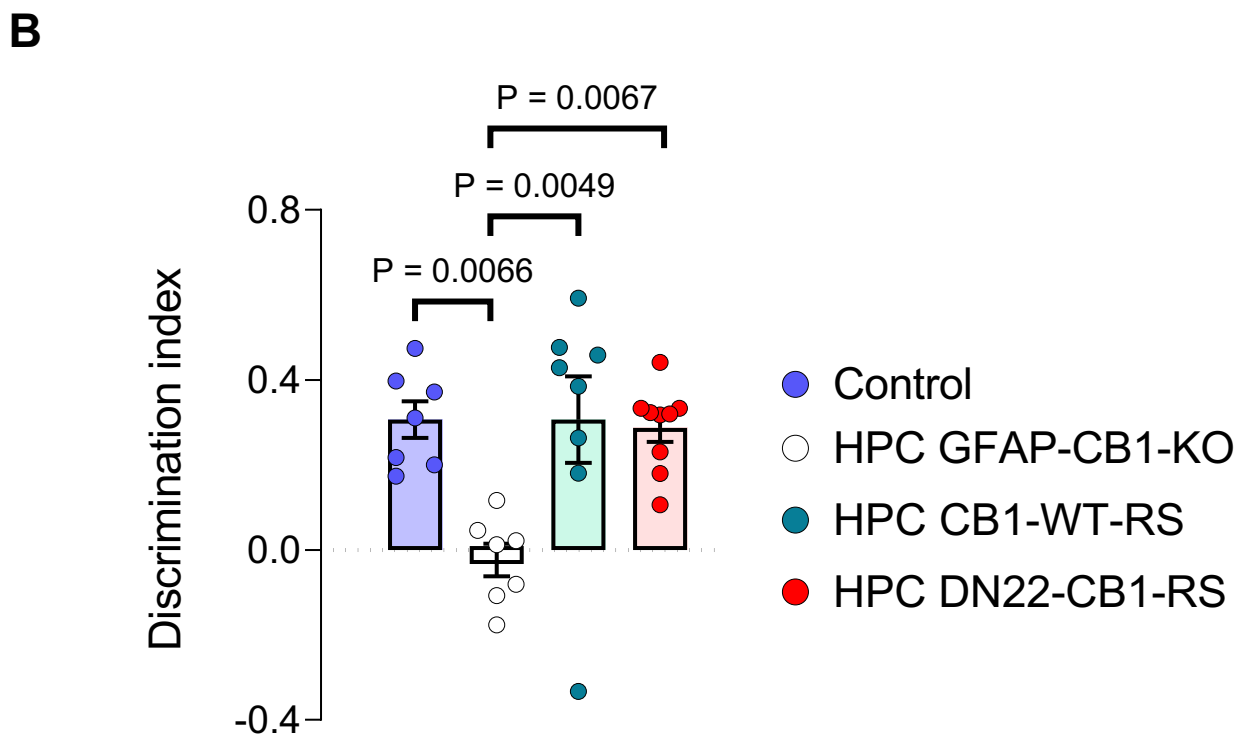

Fernandez-Moncada et al Figure 3

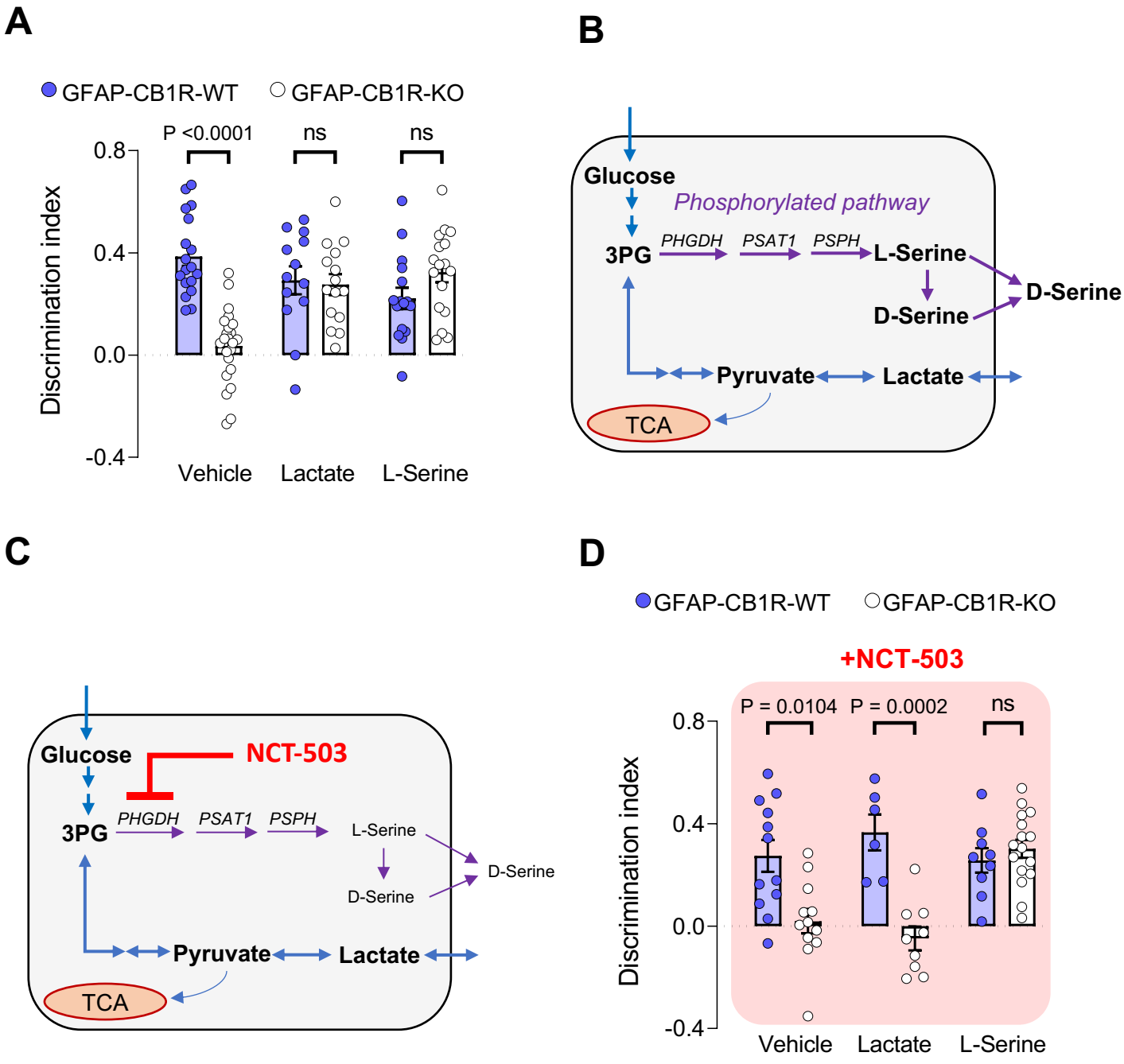

Fernandez-Moncada et al Figure 4

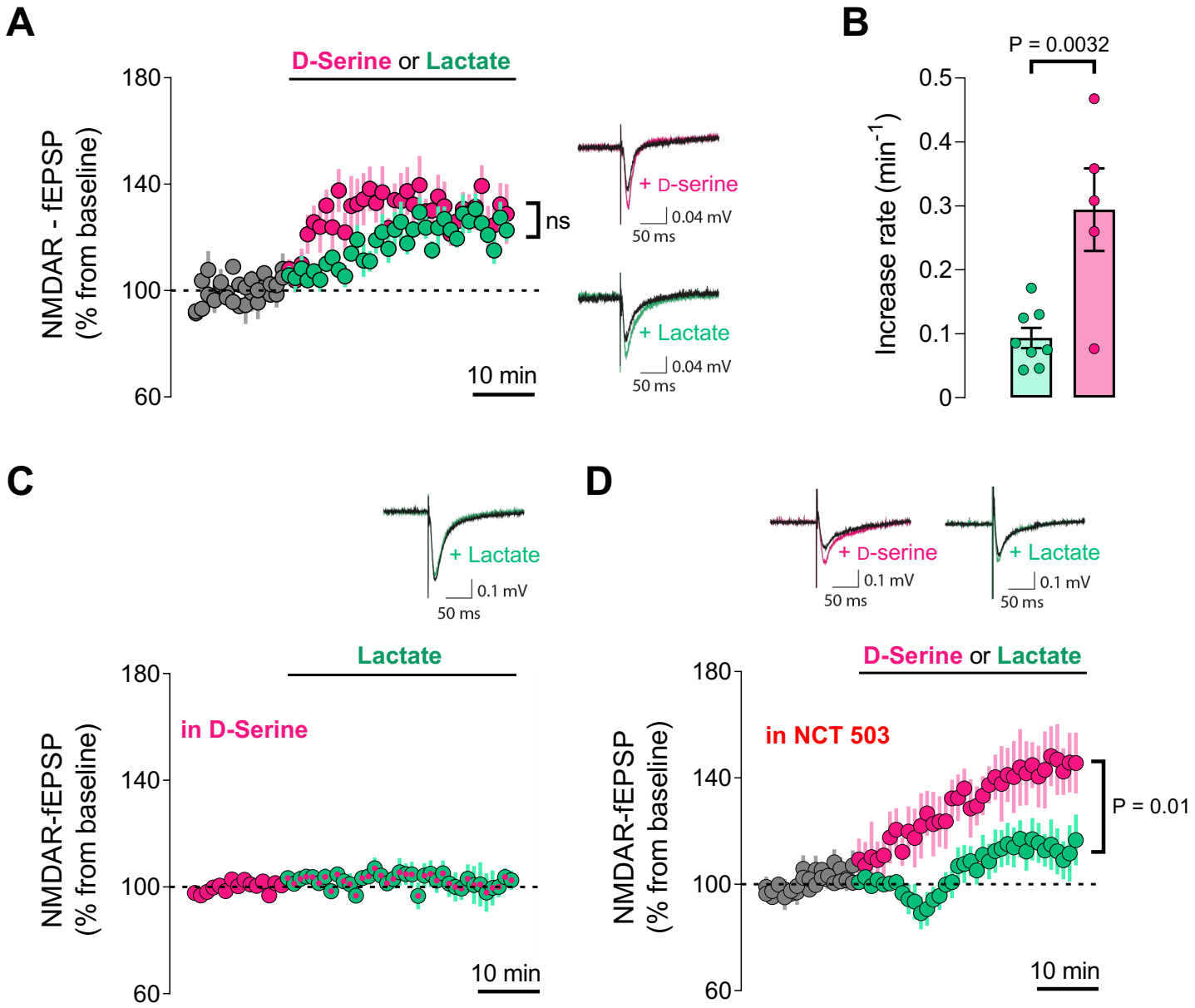

Fernandez-Moncada et al Extended Data Figure 1

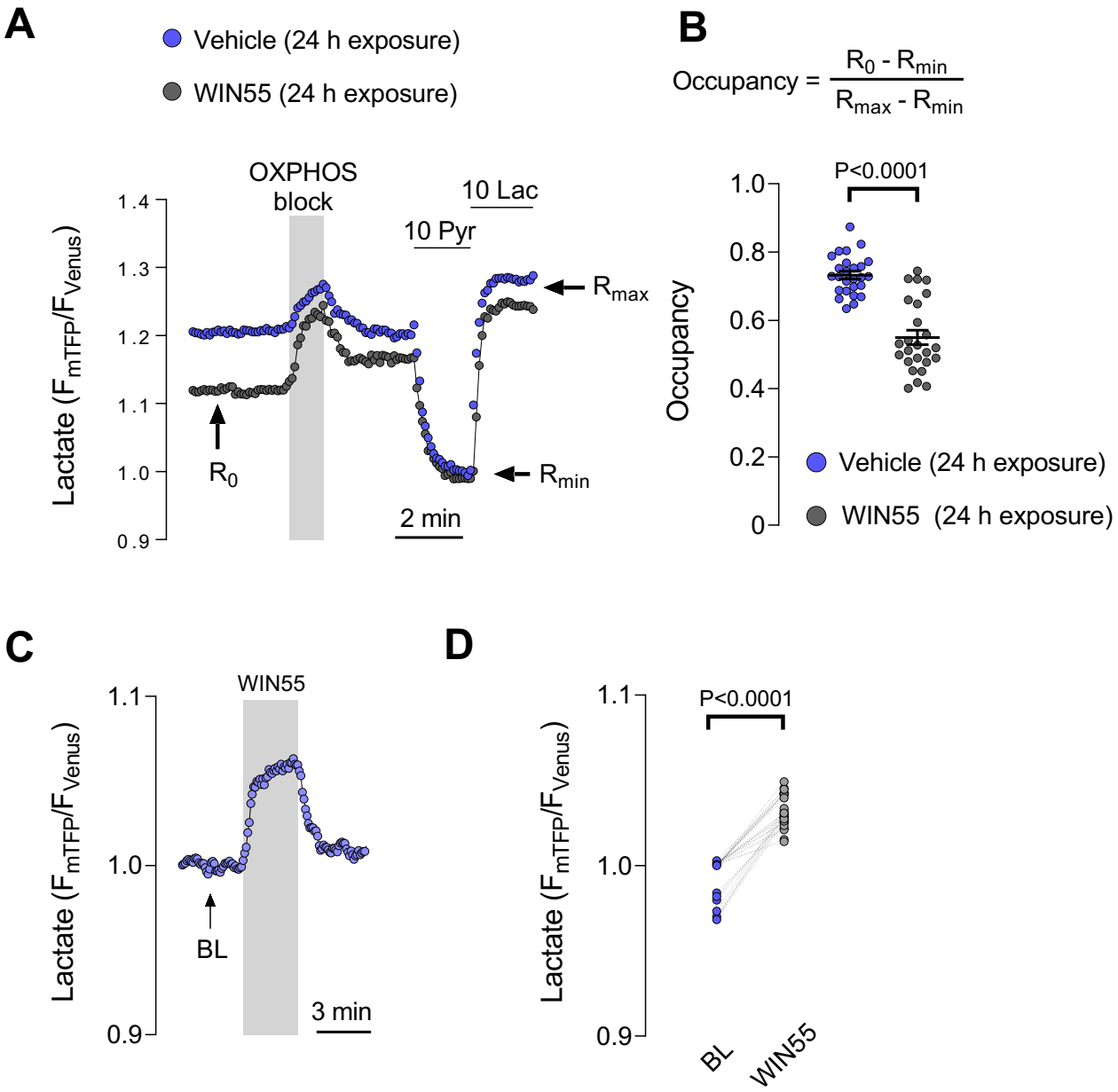

Fernandez-Moncada et al Extended Data Figure 2

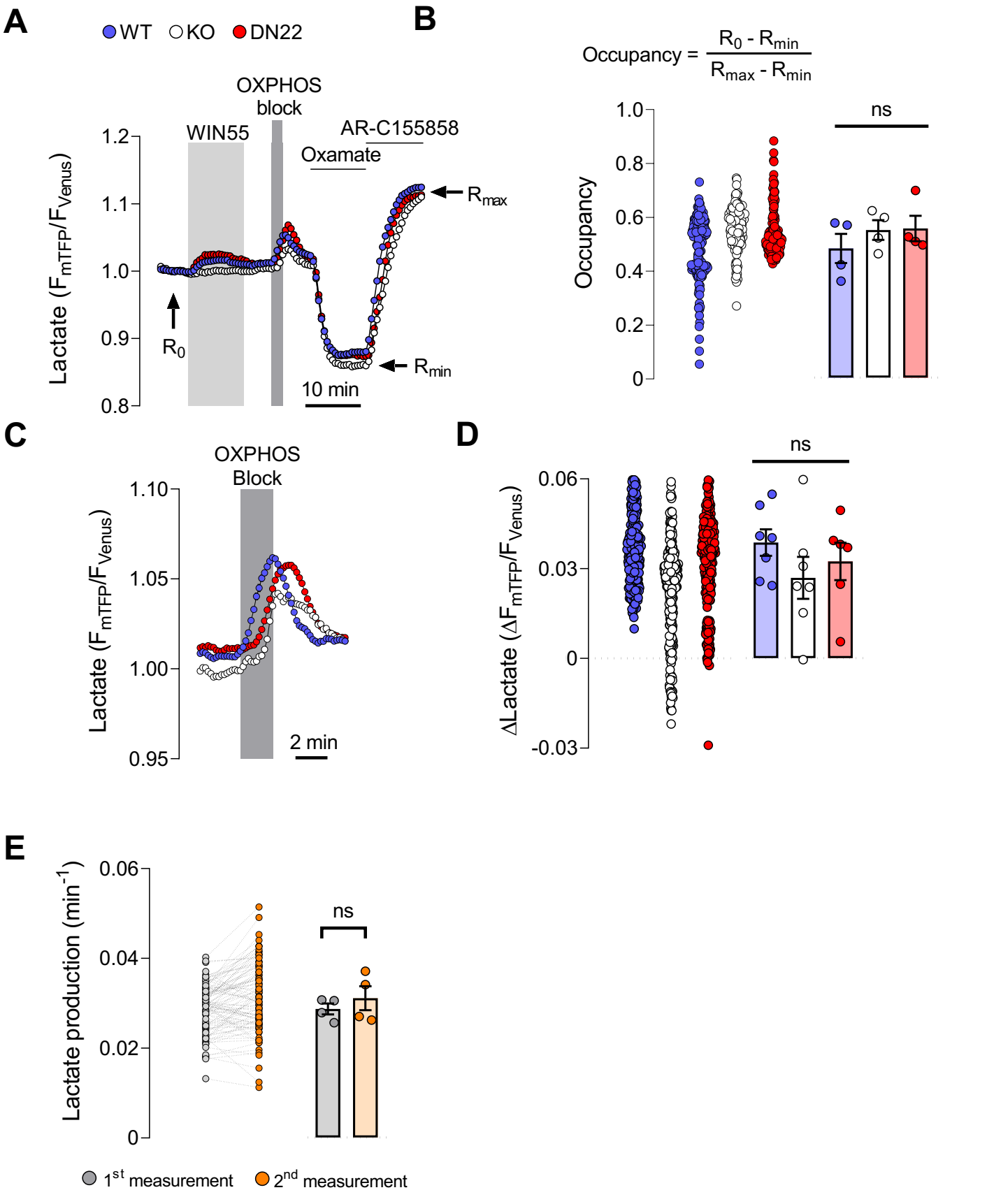

Fernandez-Moncada et al Extended Data Figure 3

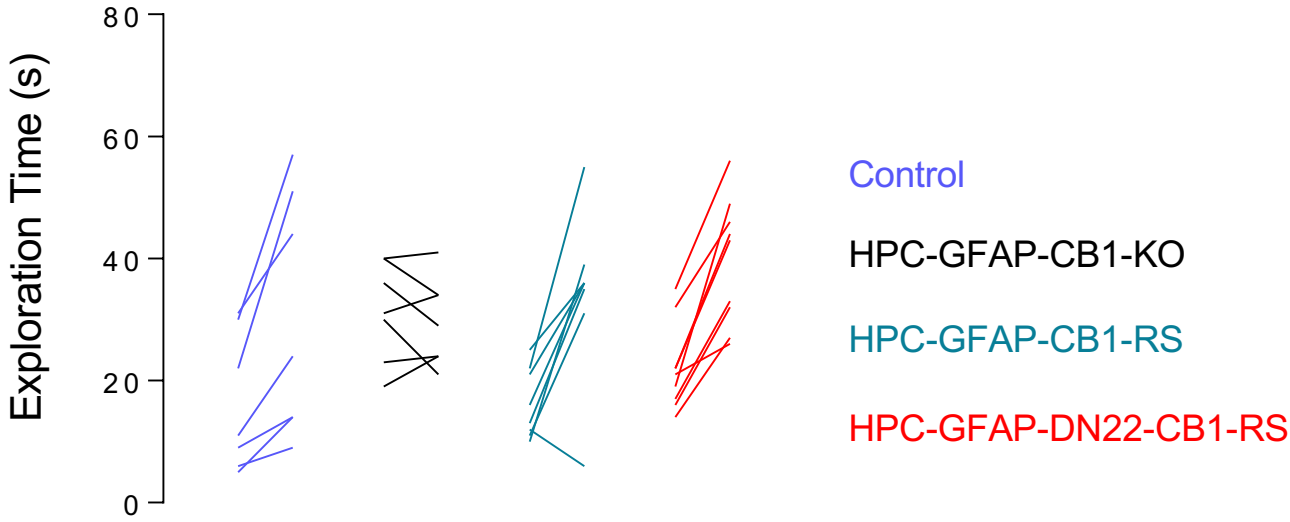

Fernandez-Moncada et al Extended Data Figure 4

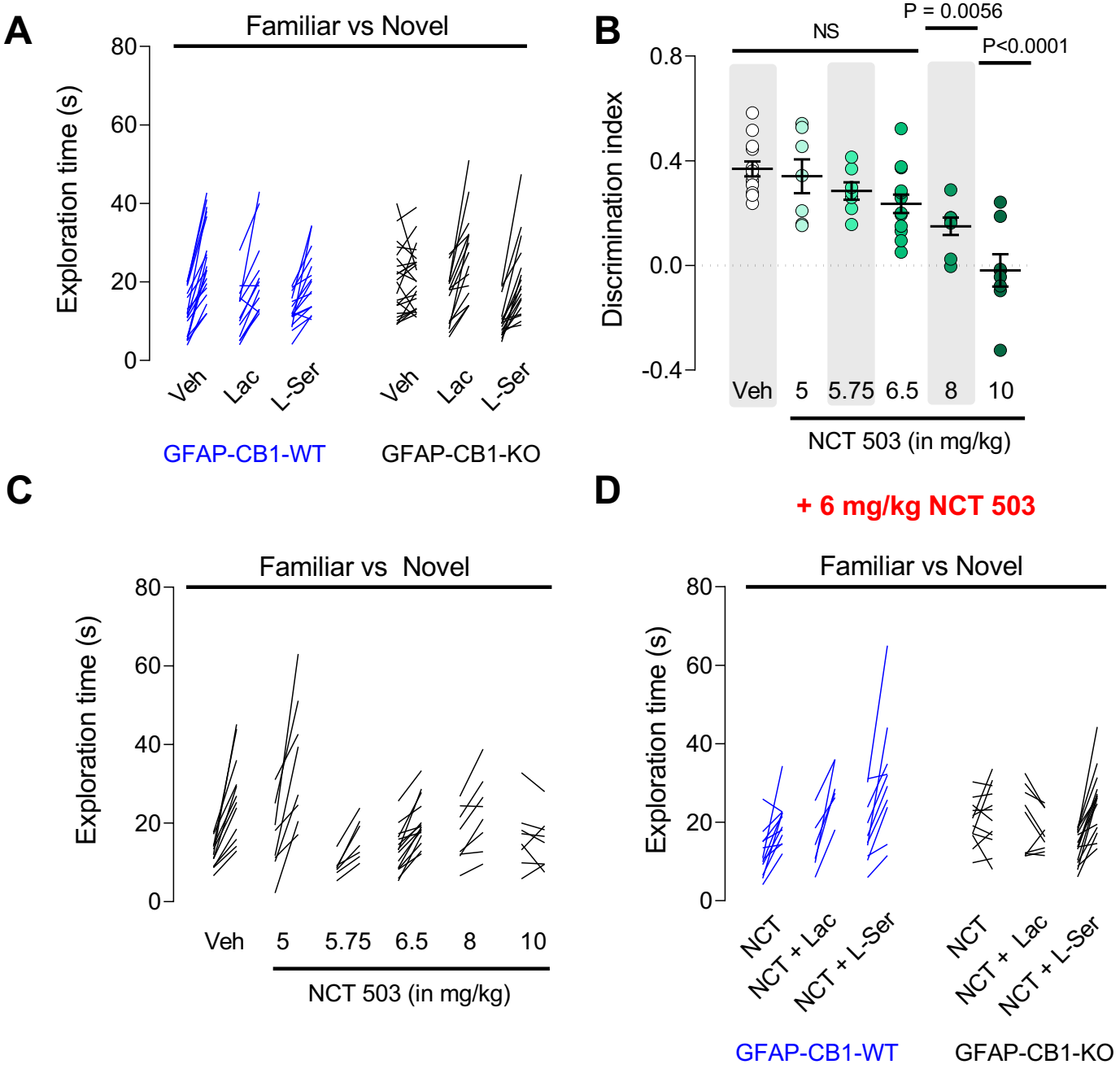

Fernandez-Moncada et al Extended Data Figure 5